Atmos. Chem. Phys. Discuss., 10, 16307–16344, 2010
www.atmos-chem-phys-discuss.net/10/16307/2010/
doi:10.5194/acpd-10-16307-2010

Atmospheric Chemistry and Physics Discussions

A very high-resolution global fossil fuel CO_2 emission inventory derived using a point source database and satellite observations of nighttime lights, 1980–2007

T. Oda and S. Maksyutov

Center for Global Environmental Research, National Institute for Environmental Studies, Tsukuba 305-8506, Japan

Received: 26 February 2010 – Accepted: 14 June 2010 – Published: 1 July 2010

Correspondence to: T. Oda (oda.tomohiro@nies.go.jp)

Published by Copernicus Publications on behalf of the European Geosciences Union.

Abstract

Emissions of CO_2 from fossil fuel combustion are a critical quantity that must be accurately given in established flux inversion frameworks. Work with emerging satellite-based inversions requires spatiotemporally-detailed inventories that permit analysis of regional sources and sinks. Conventional approaches for disaggregating national emissions beyond the country and city levels based on population distribution have certain difficulties in their application. We developed a global 1 km×1 km fossil fuel CO_2 emission inventory for the years 1980–2007 by combining a worldwide point source database and satellite observations of the global nightlight distribution. In addition to estimating the national emissions using global energy consumption statistics, emissions from point sources were estimated separately and were spatially allocated to exact locations indicated by the point source database. Emissions from other sources were distributed using a special nightlight dataset that had fewer saturated pixels compared with regular nightlight datasets. The resulting spatial distributions differed in several ways from those derived using conventional population-based approaches. Because of the inherent characteristics of the nightlight distribution, source regions corresponding to human settlements and land transportation were well articulated. Our distributions showed good agreement with a high-resolution inventory across the US at spatial resolutions that were adequate for regional flux inversions. The inventory will be incorporated into models for operational flux inversions that use observational data from the Japanese Greenhouse Gases Observing SATellite (GOSAT).

1 Introduction

Inventories of carbon dioxide (CO_2), which is a major greenhouse gas produced by humans, are a basic tool for monitoring compliance with the guidelines for managing national and global CO_2 emissions, and for the analysis of emission sources and trends in development. Analysis provides quantitative insights into fossil fuel CO_2 emissions

ACPD
10, 16307–16344, 2010

and facilitates the assessment of practical measures for emission reduction, as well as informing future projections related to socioeconomic trends. Inventory monitoring of CO_2 is conducted by the US Department of Energy Carbon Dioxide Information Analysis Center (CDIAC), which maintains a continuous archive of global emission data and monitors the 20 top-emitting countries' fossil fuel CO_2 emissions (1751–2006) (e.g., Marland et al., 2008). The International Energy Agency (IEA, http://www.iea.org/) also collects national CO_2 emission data, and the statistics cover fossil fuel CO_2 emissions in more than 140 countries and regions worldwide (1971–2005), by sector and by fuel type (IEA, 2007). National inventory datasets are often available in gridded form (e.g., Andres et al., 1996; Brenkert, 1998; Olivier et al., 2005) (typically at 1° resolution) and are used as input data for physical models, such as Global Climate Models (GCMs) and atmospheric chemical transport models (CTMs), that simulate the state of atmospheric CO_2 in both diagnostic and prognostic ways (e.g., IPCC, 2007). CO_2 flux inversions, for example, are commonly used to quantitatively estimate surface CO_2 sources and sinks at the continental scale using a combination of atmospheric CO_2 observations and transport simulations (e.g., Gurney et al., 2002; Baker et al., 2006; Stephens et al., 2007). Flux inversions, which search for the optimal balance between sources and sinks that is consistent with observations, require a priori knowledge of fossil fuel CO_2 emissions as well as knowledge of biospheric exchange and oceanic fluxes. In most of the common inversion frameworks, fossil fuel emissions are assumed to be known quantities, and only biospheric and oceanic fluxes are corrected via optimization (e.g., Gurney et al., 2002). Thus, fossil fuel CO_2 emissions are important as a reference for analyzing a budget of the three fluxes (fossil fuel CO_2 emissions, and biospheric and oceanic fluxes). Gurney et al. (2005) suggested that a potential bias occurs in flux estimates obtained by flux inversions in the case that poorly articulated fossil fuel CO_2 emission estimates are used as a priori information. Beyond established flux inversions, recent studies have indicated that flux inversions may be performed at finer spatial resolution using satellite-observed CO_2 concentrations (e.g., Rayner and O'Brien, 2001; Houweling et al., 2005; Chevallier et al., 2007). Currently,

ACPD
10, 16307–16344, 2010

several satellites monitor CO_2 levels. CO_2 concentration data are available from the Atmospheric Infrared Sounder (AIRS) satellite (e.g., Strow and Hannon, 2008) and the Japanese Greenhouse Gases Observing SATellite (GOSAT) (e.g., Yokota et al., 2009), although much care is required in adapting these datasets to flux inversions (Chevallier et al., 2005). Thus, development of a spatiotemporally detailed inventory is a key requirement for emerging satellite inversion approaches.

In constructing a gridded global emission map using national emissions, the geographical distributions of emissions have been approximated using, for example, the correlation between CO_2 emissions and population density (e.g., Andres et al., 1996; Brenkert, 1998; Olivier et al., 2005). The distribution of populations is an appropriate measure of human activity at the spatial scales of countries and states (typically 1° resolution), making it theoretically useful for describing CO_2 emission distributions. Consequently, these data provide a reasonable approximation of CO_2 emissions on these spatial scales.

However, at spatial resolutions finer than the country and state levels, population statistics cannot fully explain the spatial characteristics of potential sources. In particular, power plants and land-based modes of transport are important sources, but are usually poorly correlated with the population distribution. In addition, population statistics cannot be used to pinpoint the exact locations of potential sources, because such data (e.g. census data) usually indicate a statistical number for a certain unit area. Thus, population statistics provide only diffuse approximations of the spatial distribution of potential source regions at fine spatial scales. Furthermore, because human settlements do not have a uniform density within a region (even in a spatial unit for statistical data collection), emissions depicted at a finer scale using population statistics may be distributed in areas where people do not actually reside, and vice verse. Recently, EC-JRC/PBL (2009) developed a global 0.1°×0.1° (10 km×10 km) spatial resolution inventory, EDGAR v4.0 (the Emission Database for Global Atmospheric Research), using geographical information such as point source locations and road networks in addition to population data.

ACPD
10, 16307–16344, 2010

To achieve such fine spatial resolution, satellite observations of nightlight data have been identified as being potentially useful. The nightlight data provide a global spatial distribution of the persistent lights on the Earth's surface, thereby providing a detailed map of human activities, such as human settlements, gas flares, fires, and boats that produce strong and persistent lights (mainly squid-fishing boats) (e.g., Elvidge et al., 1997). The advantage of employing nightlight distribution over the population distribution is that it indicates the exact locations and extents of human settlements. Recently, nightlight-based global CO_2 emission maps have been developed (Doll et al., 2000; Rayner et al., 2010). However, the use of nightlight data is limited by several factors. For example, the correlation between nightlight and human activity (and hence CO_2 emissions) is only strong in developed countries (e.g., Raupach et al., 2009). In addition, such data do not accurately indicate the variability in intensity of emissions from power plants and other point sources without additional information, although they do pinpoint or approximate the exact locations of these sources.

For the US, these difficulties (including descriptions of temporal variations of emissions in addition to spatial patterns, which is another source of uncertainty that may significantly influence the model results) have been overcome by Gurney et al. (2009). The *Vulcan* project (www.purdue.edu/eas/carbon/vulcan) based its development on a fine-scale inventory (10 km×10 km) compiled by individual source sectors (Gurney et al., 2009). Furthermore, research into a more detailed fossil fuel CO_2 inventory, called *Hestia* (www.purdue.edu/climate/hestia), has been conducted for the city of Indianapolis in a pilot study. Using a combination of in situ measurements, remote sensing, and energy systems modelling, Hestia will provide a building-scale fossil fuel CO_2 inventory in near-real-time (Gurney et al., 2009). The Vulcan approach could be applied at the regional scale using the wealth of detailed information that is potentially available, but this method is difficult to apply on the global scale because of a lack of data.

In this study, we developed a global high-resolution annual emission inventory, ODIAC (Open source Data Inventory of Anthropogenic CO_2 emission), for the years 1980–2007. The primary goal of developing the ODIAC inventory is to provide a priori

ACPD
10, 16307–16344, 2010

information on fossil fuel CO_2 emissions for regional flux inversions using GOSAT observational data. This inventory was developed by making use of a point source database and satellite nightlight data. National emissions were estimated using global fuel consumption statistics, and emissions from power plants were calculated using the point source database. Point sources were mapped to exact locations using the coordinate information available in the point source database, and the spatial distribution of the residual emissions (total emissions minus point source emissions) was determined using the nightlight data. Because nightlight data are provided at a resolution of 30 arc seconds (approximately 1 km), CO_2 emissions can also be mapped at this resolution.

In developing this inventory, the primary focus was disaggregation of national emissions at a finer spatial scale by combining the point source database and the satellite nightlight data. In the sections that follow, we explain how the inventory was constructed and discuss its inherent limitations. Herein, the terms fossil fuel (and anthropogenic) CO_2 emissions refer to emissions over land, which are attributable to the combustion of fossil fuels (coal, oil, and natural gas). Non-land fossil fuel CO_2 emissions from sources such as international bunkers (marine and aviation) and fisheries, which are usually not correlated with the nightlight distribution, were included in the land emissions estimates. Although gas flare emissions could be pinpointed using the nightlight data, they were incorporated into the land emissions because it was not appropriate to distribute those distinct emissions together with other aggregated land emissions. The emissions that were not considered herein may be introduced using supplemental existing inventories, such as EDGAR v4.0 (EC-JRC/PBL, 2009) for international bunkers and global gas flare estimates by the US National Oceanic and Atmosphere Administration (NOAA) (http://www.ngdc.noaa.gov/dmsp/interest/gas_flares.html).

ACPD
10, 16307–16344, 2010

2 Data and methodology

Development of this inventory was performed in a stepwise manner, as discussed below.

2.1 National and regional CO_2 emissions

Estimates of annual national CO_2 emissions obtained in this work were based on worldwide energy statistics (2007 edition) compiled by the energy company BP p.l.c. (BP, 2007). The BP energy statistics were recently used to extend the established historical emission inventories (e.g. CDIAC) prior to updating the original inventories (e.g., Gregg et al., 2007; Myhre et al., 2009). The 2007 edition of the BP statistics, which covered the years 1965–2007, included the consumption of commercially-traded primary fuels (e.g. oil, coal, and natural gas) in 65 countries and administrative regions (see Table 2). Consumption of such fuels in six major geographical regions (North America, South and Central Americas, Europe and Eurasia, the Middle East, Africa, and Asia Pacific) was also provided to show the statistics in countries or regions that were not included in BP (2007). The definitions of geographical regions are summarized in Table 1.

Annual total CO_2 emissions for 71 regions (65 nations and regions as well as the 6 major regions) were calculated from the consumption statistics for oil, coal, and natural gas. The oil statistics indicated all inland consumption, international airborne and maritime transport, and refinery fuel production and losses. Consumption of fuel ethanol and biodiesel were also included. The coal statistics in BP (2007) included the quantities of solid fossil fuels, such as bituminous coal, anthracite (hard coal), lignite, and brown (sub-bituminous) coal.

The CO_2 emissions were estimated by calculating the carbon content of the consumed fuels. Our estimation procedure paralleled the methodology specified in the revised IPCC 1996 guidelines for the national greenhouse gas inventories (IPCC, 1996), except in the estimation of national fuel consumption. The reference approach of the revised 1996 IPCC guidelines specified that the amount of total fuel supplied, which

ACPD
10, 16307–16344, 2010

was correlated with the apparent consumption, formed the basis of calculations of national carbon supply, and the amount was calculated as the sum of the produced and imported quantities, minus the quantities attributable to international bunkers and stock changes. National emissions, as defined earlier, were calculated based on the total quantity of consumed primary fuels reported in BP (2007). The conversion factors used in the calculation were adopted from the 2007 statistics report prepared by IEA (2007), unless specified otherwise. The quantities of nationally and regionally consumed primary fuels in BP (2007) (in million tonnes of oil equivalent per year) were first converted into energy quantities (in units of Terajoules). The quantity of natural gas in BP (2007) was given in billions of cubic meters, and a conversion factor of 0.90 was applied to express this quantity in millions of tonnes of oil equivalent (Mtoe). The obtained quantities of energy were then used to compute the carbon content of the consumed fuels. The following carbon emission factors (CFE, in tonnes of carbon per Terajoule) were applied: 15.3 (natural gas); 26.4 (coal); 20.0 (oil). The CFE adopted here for coal was calculated as the average of CFEs for anthracite, coking coal, other bituminous coal, sub-bituminous coal, and lignite. To account for the fraction of carbon that was not oxidized in the combustion of the fuels, correction factors of 0.99 (oil), 0.98 (coal), and 0.995 (natural gas) were applied. The annual estimates for the national/regional CO_2 emissions from primary fuel combustion were then found by multiplying the remaining carbon quantities by 44/12, which is the molecular weight ratio of CO_2 to carbon.

National and regional annual total emissions were calculated for the years 1980–2007. BP (2007) did not report quantities smaller than 0.05 (in million tonnes of oil equivalent per year) in their statistics; therefore, those quantities were assumed to be 0.05. The consumption statistics for the eight former Soviet Union countries (Azerbaijan, Belarus, Kazakhstan, Lithuania, Russian Federation, Turkmenistan, Ukraine, Uzbekistan) prior to 1985 were unavailable, and, therefore, were extrapolated by scaling to the annual total consumption for the full former Soviet Union provided in BP (2007).

ACPD
10, 16307–16344, 2010

2.2 CO_2 emissions from point sources

In addition to national and regional emissions, we separately estimated emissions from point sources using a global power-plant database. We utilized the database CARMA (Carbon Monitoring and Action, http://carma.org), which was compiled using data from national publicly disclosed databases for the US, EU, Canada, and India, and a commercial database of the worlds power plants (Wheeler and Ummel, 2008). The database included emission levels and locations of over 50 000 power plants worldwide for the years 2000 and 2007, including all types of power plants (fossil fuel, nuclear, hydro, and other renewable energy plants). Data for the fossil fuel-fired power plants with valid location information (n=17 668) were selected from the database, and the values for the national total emissions from such power plants were calculated. Emissions of individual power plants were assigned to the locations indicated by CARMA.

We used data for the year 2007 to extend the emission estimation to the entire period of interest (1980–2007). The 17 668 power plants were assumed to be operational during this period, and their annual emission levels were simply scaled by the national (or regional) emission trends obtained from BP (2007). In practice, the emissions for the year 2007 were used to account for the emissions for the year 2006. Emission data available in the CARMA database were derived by compiling and analyzing the data from different years, such as the eGRID database (http://www.epa.gov/cleanenergy/energy-resources/egrid/index.html); therefore, a 1-year shift in the base year did not critically affect the results.

The global spatial distribution of power plants used in this study is shown in Fig. 1. High concentrations of power plants can be seen in major emitting countries, such as the US, European countries, India, China, and Japan. In particular, power plants that generated emissions exceeding 15 Mt CO_2/yr (4 Mt C/yr), which were ranked as the top 100 emitting power plants in CARMA, were located mainly in these countries. In the Southern Hemisphere, power plants of similar size were sparsely distributed across South America, South Africa and the east coast of Australia. A scattering of

ACPD
10, 16307–16344, 2010

relatively small power plants can be seen across Africa. By making use of the CARMA database, the spatial features of the power plant distribution were directly included in our inventory.

2.3 CO_2 emissions from other sources and their spatial distribution

Emissions from power plants were estimated using the CARMA database; thus, emissions from other sources (often denoted as non-point sources) in a country (or a region) were loosely approximated by subtracting the emissions of power plants from the national (or regional) total emission distributions. The non-point sources include industrial, residential, and commercial sectors, as well as daily land transportation. Emissions from these sources could be diffuse and were not as strong or as persistent as emissions from the point sources. This approximation can be useful in globally analyzing the locations and strengths of non-point sources using a surrogate distribution. A surrogate commonly fails to distinguish point source from non-point source emissions. Both emission types are equally distributed, although point sources are commonly poorly correlated with human activities. With the approximation described above, we employed a surrogate to explain only the non-point emissions.

The spatial distribution of non-point sources was determined using data from the satellite nightlight observations. The original nightlight data were obtained from the US Air Force Defence Meteorological Satellite Project Operational Linescan System (DMSP-OSL) satellites. The US National Oceanic Atmospheric Administration (NOAA) National Geophysical Data Center (NGDC) maintains the data archive, and the digital archives of standard products are available for 1997–2003. DMSP-OSL satellites are in sun-synchronous polar orbits (altitude=830 km above the surface) and provide global coverage twice per day. The broadband visible–near infrared channel (0.4–1.1 µm), with intensification by a photomultiplier tube (PMT) in the night time, detects the clouds illuminated by moonlight as well as nightlight. Nightlight data have been used to map human settlements (Elvidge et al., 1997, 1999), gas flares (Elvidge et al., 2001), and populations (Briggs et al., 2007), as well as mapping CO_2 emissions (Doll et al., 2000;

ACPD
10, 16307–16344, 2010

Rayner et al., 2010). It is known that intense lights such as city lights and gas flares cause instrumental saturation due to the high sensitivity of the instruments required for cloud detection. Because the radiance levels in saturated pixels are truncated, it is generally difficult to use nightlight data for mapping emissions across bright regions. Recently, Rayner et al. (2010) developed a data assimilation system for fossil fuel CO_2 emissions, FFDAS (Fossil Fuel Data Assimilation System). FFDAS is based on an extended Kaya identity, producing global emission fields by assimilating nightlights data together with other data such as population data that constrain the Kaya identity model. Rayner et al. (2010) compensated for such saturation using a correction equation derived from the probabilistic analysis presented by Raupach et al. (2009).

In this study, instead of correcting for saturation, the "radiance calibrated lights" data (data available from http://www.ngdc.noaa.gov/dmsp/download_rad_cal_96-97.html) were applied as a surrogate. The "radiance calibrated lights" were obtained from special measurements acquired in a reduced-gain (low-sensitivity) mode in 1996 and 1997. This dataset has fewer saturated pixels compared with the datasets obtained by normal measurements (Elvidge et al., 1999; Cinzano et al., 2000). Cinzano et al. (2000) used the calibrated radiance data to construct a map of the night sky brightness. The data have a resolution of 30 arc second (approximately 1 km) and are provided as 2-year composite data. Raw data at pixel resolution are provided in digital number (DN) format across the range 0–255, where 0 signifies that no lights were observed at a location during the observation period and 255 indicates a saturated pixel. DNs between 1 and 254 were valid and could be converted into a radiance quantity using a conversion equation. Here, we replaced DN 255 with 254 for simplicity. Consequently, emissions at pixels assigned a DN of 254 may be underestimated. As described earlier, we do not consider emissions from gas flares in this study. The pixels corresponding to gas flares were identified using a worldwide dataset of gas flares in 2004, developed by Elvidge et al. (2007), and were then eliminated.

ACPD
10, 16307–16344, 2010

2.4 Data integration

Annual gridded emission inventories were developed by combining emission estimates of point sources and non-point sources. Point source emissions were placed directly at exact locations using coordinate information (latitude and longitude) available in the CARMA database. National (or regional) total emissions from non-point sources were distributed to 1 km×1 km pixels according to the distribution of nightlight radiance. The distribution was formed by superimposing the nightlight data and national boundary data, which were used to identify the national attributes of pixels. Radiance quantities across all pixels attributed to a country (or a region) were summed, and the original quantity at each pixel was normalized by the national (or regional) sum. The CO_2 emission intensity at a pixel was scaled by multiplying the normalized radiance with the annual total emission of a country or a region. We used 2.5 arc minute (approximately 5 km) national boundary data (year 2000) of the Gridded Population of the World version 3 (GPWv3), developed by the Center for International Earth Science Information Network at Columbia University, NY, USA (data available from http://sedac.ciesin.columbia.edu/gpw/global.jsp). Boundaries between land and ocean, river, and water bodies (e.g. coastline) were defined using IGBP land-cover classification data of the NASA TERRA/MODIS HDF-EOS MOD12Q1 V004 product (data available from http://duckwater.bu.edu/lc/mod12q1.html) (e.g., Belward et al., 1999). Pixels with DN of 0 (indicating water) were considered to be non-land pixels. In addition, pixels with DN of 254 (indicating unclassified) that were apparently located in ocean, river, and water bodies were included as non-land pixels.

A gridded inventory (ODIAC) for the years 1980–2007 was developed using the procedure described above. Due to the fine resolution of the nightlight data, the original ODIAC datasets for each individual year were rather large (approximately 3.5 GB). For convenience in data handling, we developed a 2.5 arc minute (5 km) low-resolution inventory. The analysis described in this paper was obtained from the low-resolution inventory dataset unless stated otherwise. The low-resolution inventory was developed

ACPD
10, 16307–16344, 2010

using 2.5 arc degree nightlight data reduced from the original 30 arc second (1 km) dataset.

3 Results and discussion

3.1 Global, national, and regional annual CO_2 emissions

The estimates for national and regional annual CO_2 emissions for the year 2006 are presented in Table 2. The global total CO_2 emission for the year 2006 was estimated to be 29 992 Mt CO_2/yr (8172 Mt C/yr). In our estimate, the US was initially the country contributing the largest fraction of emissions (6411 Mt CO_2/yr, equivalent to 1746 Mt C/yr) and remained the world's emissions leader until the year 2007. The second-largest emitter was China (6023 Mt CO_2/yr, 1641 Mt C/yr). Recently, Gregg et al. (2007) suggested that China has led the world in emissions since late 2006. The conclusions of Gregg et al. (2007) differed from ours, possibly because we used energy statistics which is different from the one CDIAC used and employed a rather simple method for calculating the national emission estimates. Other prominent emitting countries were the Russian Federation (1681 Mt CO_2/yr, 458 Mt C/yr), Japan (1371 Mt CO_2/yr, 374 Mt C/yr), and India (1220 Mt CO_2/yr, 332 Mt C/yr); these five countries accounted for 56% of the global total CO_2 emissions, according to our estimations.

The national emission levels for other countries and the fraction of point source and non-point source emissions are shown in Fig. 2. Global total CO_2 emissions from power plants were estimated to be 10 246 Mt CO_2/yr (2792 MtC/yr), which is 34% of our global total CO_2 emission estimate. Here, we note that the emissions from all power plant data available in CARMA were not summed, because invalid power plant data were eliminated at an earlier stage of the analysis. At national and regional levels, CO_2 emissions from point sources may account for a substantial proportion of the total emissions. Emissions from point sources contribute to approximately half of the total emissions in Australia (47.9%), Bulgaria (47.9%), China (51.8%), the Czech Republic (50.0%), Germany (48.1%), Finland (51.9%), Greece (47.1%), India (52.2%),

ACPD
10, 16307–16344, 2010

the Philippines (50.7%), Poland (54.5%), and South Africa (48.5%). Because the use of just one of the common surrogates alone (e.g. nightlight or population) does not generally explain intense point source emissions, inclusion of point sources might be practical and offer a reasonable method for determining the spatial emission patterns. Single use of a surrogate may underestimate point source emissions and overestimate non-point sources, especially when one expects to look at finer spatial scales. Because the six major geographical regions are aggregated categories of countries and regions that are not included in BP (2007), we assumed that the countries and regions within each major region had the same fraction of CO_2 emissions from point sources and non-point sources. The fraction of total emissions from point sources appeared to be smaller than the fraction of emissions from point sources in 61 countries and regions. This discrepancy may result from the fact that most industrial countries and regions were included in the 61 countries and regions. However, CO_2 emissions from point sources in the six geographical regions may still account for a considerable fraction of the total emissions.

To quantify the deviations from emission estimates in previous studies, we compared our global and national estimates with a wide variety of inventories, such as CDIAC (Boden et al., 2009), IEA (IEA, 2007), and EDGAR v4.0 (EC-JRC/PBL, 2009), which were developed using a variety of procedures (Fig. 4). The data, calculation methods, and CEFs differed in each of the inventories listed above, and deviations from these estimates were expected. Briefly, national total emissions from CDIAC, for example, were estimated using the apparent consumption distribution and were based on energy statistics published by the United Nations (UN, 2008) (e.g., Marland and Rotty, 1984). On the other hand, global total emissions from CDIAC were estimated using production statistics based on UN (2008) (e.g., Marland and Rotty, 1984). CDIAC estimates for the comparison are the summation of emissions from the combustion of fuels (gas, liquid, and solid) and gas flaring; emissions from cement production are not included. The calculation procedure utilized by IEA paralleled the methodology shown in the revised IPCC 1996 guidelines (IPCC, 1996) (IEA, 2007). IEA provided two types of estimates:

ACPD
10, 16307–16344, 2010

a *reference approach* and a *sectoral approach*. The reference approach began with a calculation of the apparent consumption using the sectoral approach, and national estimates were developed by compiling reported national sectoral emissions. In the IPCC framework, a reference approach was used to verify the inventory developed using a sectoral approach. For comparison, we selected estimates that used the sectoral approach, based on a procedure that differed from ours. IEA emissions obtained using the sectoral approach presented in this study are solely attributable to the combustion of fossil fuels, which are categorized as IPCC source category 1A (fuel combustion). In EDGAR v4.0, national emissions were calculated using country- and technology-based data organized by sector, which was specified in the IPCC guidelines, and also using country-specific emission factors (EC-JRC/PBL, 2009). The national sectoral emissions were placed on a 0.1 arc degree (approximately 10 km) spatial grid using spatial distributions of population, point sources, and road networks. The EDGAR v4.0 global emissions reported in this paper represent the sum of emissions attributable to IPCC source category 1A. For national emissions, emissions from industrial processes (e.g. cement production) are included.

As shown in Figs. 3 and 4, the global total emissions in this study overestimated other reported inventories. For the year 2005, in which estimates from all four studies are available, the global CDIAC estimate was 28 079 Mt CO_2/yr (7651 Mt C/yr), IEA was 27 136 Mt CO_2/yr (7394 Mt C/yr), and EDGAR v4.0 was 25 678 Mt CO_2/yr (6997 Mt C/yr), whereas our estimate was 29 130 Mt CO_2/yr (7937 Mt C/yr). Of the three compared inventories, our estimate showed the best agreement with the CDIAC estimate (our estimates were on average 4% higher than the CDIAC estimates). This was probably due to the fact that the calculation methods for estimating the national emission levels in the CDIAC estimate were similar to ours, whereas the other two inventories were based on different calculation methods. Our estimate overestimated emissions relative to IEA and EDGAR v4.0 for all years in the period of interest (the average difference in annual emissions was 8% and 13%, respectively).

Figure 4 compares the historical emission estimates for the top five emitting countries

ACPD
10, 16307–16344, 2010

(the US, China, Russia, India, and Japan). The annual national emission trends in this study agreed well with those of other studies, although quantitative differences between the annual emissions were present. The differences arose from the same factors that contributed to differences in the global estimates. At the national level, in particular, the deviations from other estimates may be more apparent than at the global emission level, because the data, calculation methods, and emission factors used in the other three studies were usually country-specific. For example, the calculation method in the CDIAC estimate was based on apparent consumption, as described, whereas the national emissions in this study were derived from the annual total fuel consumption. Thus, deviations from the CDIAC estimate at the national level may be explained by, for example, the omission of adjustments for import/export and stock change. The average deviation from the CDIAC US estimate was 11.7% (see Fig. 4a). Our estimates for China (Fig. 4b) and India (Fig. 4d) were reasonably close to other estimates. For the Russian Federation (Fig. 4c), our estimates were within the inter-inventory differences post-1991; however, our estimates did not agree with the emission trends shown in EDGAR v4.0 prior to 1991. This may reflect differences in the data used for estimating national emissions.

3.2 Spatial distribution of CO_2 emissions at the global, regional, and city-level scales

3.2.1 Global scale

The spatial distribution for the gridded global CO_2 emissions during the year 2006 is shown in Fig. 5. CO_2 emissions in Fig. 5 are expressed as the log (base 10) of tonnes of carbon per cell (5 km×5 km) per year. Point source emissions imported from the CARMA database were directly placed in the exact locations indicated by CARMA, but this spatial distribution, which can be seen in Fig. 1, was not apparent in the global distribution, even though it was based on reduced 5-km resolution data. The most prominent features of the spatial distribution shown in Fig. 5 were dominated by

ACPD
10, 16307–16344, 2010

non-point source emissions, which were represented in the nightlight data. Therefore, the spatial features that were readily observable were directly inherited from the native nightlight distribution. Large concentrations of intense source areas can be seen over Eastern North America, Northern and Western European countries (e.g. UK, Belgium, and the Netherlands), and East Asian countries (e.g., India, China, South Korea, and Japan), especially in the Northern Hemisphere, where many intense lights can be observed. In the Southern Hemisphere, in contrast, massive source regions are not as prevalent as in the Northern Hemisphere, as one might expect. Although individual point sources cannot be distinguished, large metropolitan areas (e.g., Los Angeles, Chicago, Mexico City, Sao Paulo, London, Paris, Moscow, Johannesburg, Delhi, Bangkok, Shanghai, Beijing, Seoul, and Tokyo) can be identified as intense sources of millions of tonnes carbon per year. In addition, we can identify regional spatial characteristics that are depicted in detail by the nightlight distribution. For example, source regions along the interstate highway network in the US, road networks around Moscow, the Trans-Siberian Railway, the Nair, and the Indus, are visible spatial characteristics even in the global picture. Those nightlights observed using DMSP-OLS instruments may not be lights attributable exactly to the sources, and may be lights coming from nearby cities. However, the distribution may still be used as a surrogate for regional unique sources, such as area sources and line sources.

As stated above, emissions at a pixel were calculated by multiplying the national (or regional) total emissions by the ratio of the radiance level at a pixel to the national (or regional) total radiance. Therefore, if the total emissions are the same, emissions at a pixel can be overestimated in a country (or region) that has a smaller number of source region pixels according to the nightlight distribution. In fact, pixels across China indicated more intense emission levels than those in the US, whereas the total national emission levels in the US in 2006 were larger than those of China in this study. This result occurs because China includes smaller source regions than does the US, if one utilizes nightlight as the unique surrogate. The same explanation may account for the differences between physically small countries that are assigned intense

ACPD
10, 16307–16344, 2010

emission levels, such as the Netherlands, Belgium, and Japan. As seen in Fig. 5, the fine depiction of source regions could offer advantages for spatial emission mapping in countries (or regions) with physically large territories and small (or concentrated) human settlements, especially at a regional scale. Source regions indicated by population data could be diffuse due to the spatial unit used for statistical data collection, potentially resulting in the underestimation of emission intensities. Here, we assumed that the nightlight intensity was linearly and uniformly related to CO_2 emissions all over the world. The proportionality constant may actually be country-specific. Moreover, nightlight may not explain spatial variations in emissions that are attributable to differences among source sectors. Because nightlight usually correlates with human activity, it also correlates with the population distribution to a similar extent. However, the spatial distributions of nightlight and population were fairly different. As a measure of the similarities and differences, we calculated the spatial correlations and absolute differences between our inventory and the CDIAC 1°×1° gridded inventory for the year 2006 (Andres et al., 2009). Here, emissions of Andres et al. (2009) include emissions from cement production and fishery emissions that are not considered in our estimate. Because the CDIAC gridded inventory was developed at a spatial resolution of 1°, the comparison was performed at the same resolution by upscaling our emission map. The spatial correlation factor was 0.66 and the absolute difference between the two inventories was 25 332 Mt CO_2/yr (6902 Mt C/yr). The differences between the two inventories could be explained by the differences between the spatial distributions, and by emissions that were not considered in our estimate.

3.2.2 Regional scale

Figure 6 shows enlarged views of North America, Europe, East Asia, and West Asia. To determine the spatial emission patterns at the regional scale, combinations of the spatial information (e.g. industry, population, and transportation) are often used (e.g., Ohara et al., 2007; Gurney et al., 2009). In contrast, this study assumed that nightlight functioned as a comprehensive surrogate for regional sources. In fact, as shown in

ACPD
10, 16307–16344, 2010

Fig. 5, nightlight may indicate the major transportation networks (e.g. the US and Europe) in addition to human settlements. Although individual power plants were not visible at this scale, power plants had already been placed at exact locations. The detailed regional population data may work in a similar way; however, the resultant distribution may be diffuse. It is not realistic to attempt to prepare a detailed, consistent global population map because of a lack of data.

A comparison of region-focused evaluations was made by comparing our emission map with the Vulcan inventory (Gurney et al., 2009), together with the CDIAC (Brenkert, 1998) and FFDAS (Rayner et al., 2010) emission maps. The comparison was performed according to the criteria described in Rayner et al. (2010). A summary of the comparison is given in Table 3. The total emissions from the maps were scaled with respect to the Vulcan total emission level for the year 2002. The spatial correlations and absolute differences (sum of the absolute value of the Vulcan values minus the map being compared) were then calculated at different spatial scales (0.5–4°). Among the participating maps, the CDIAC map (Brenkert, 1998) was purely population-based and has been widely used in flux inversion studies (e.g., Gurney et al., 2002). As stated earlier, FFDAS produces emission fields based on an extended Kaya identity by assimilating nightlights data together with population data. Thus, FFDAS is not solely based on nightlight data, although the contribution of nightlight data is apparent in the resulting map. The produced spatial distribution of emissions is intermediate between that of nightlight-based and population-based approaches, and is more smooth than that of traditional population-based inventories (Rayner et al., 2010). FFDAS showed better agreement with Vulcan compared with emission maps based solely on population or solely on nightlight data (Rayner et al., 2010).

The comparison results demonstrate that our emission map showed the best agreement with the Vulcan map at all spatial levels (e.g. a correlation of 0.87, even at 0.5° resolution) in terms of absolute difference and spatial pattern. Assuming that the major difference between the procedures used in FFDAS and the present study is the inclusion of point sources in the present study, this factor may be crucial for emission

ACPD
10, 16307–16344, 2010

mapping at fine spatial scales. Regional agreement in spatial pattern on such spatial scales is an appealing feature for regional flux inversions, including conventional region- and grid-based types of inversions in which flux estimates are derived based on spatial patterns of a priori fluxes given as a first guess for optimization. In addition, the good quantitative agreement with the Vulcan emission maps would benefit atmospheric simulations, regardless of the fact that the comparison was performed by scaling the total emissions to the Vulcan.

3.2.3 City-level scale

Figure 7 shows the spatial distribution of CO_2 emissions at six major populated cities worldwide (Los Angeles, Sao Paulo, Moscow, Delhi, Shanghai, and Tokyo). Those maps were based on the native 30 arc second (1 km) resolution ODIAC inventory. As seen in Fig. 7, the local spatial structures of large cities were clearly depicted by the nightlight data. In addition, the spatial variability in CO_2 emission levels could be seen even in city cores, where standard measurements from the DMSP-OLS instruments usually register saturation. Those spatial distributions may be similar in appearance to those expected from a population-based method, and they may not explain the emission patterns by sector. Regardless of such limitations, however, the use of the "radiance calibrated light" data enabled us to indicate possible source regions at good spatial resolution and offers a practical method for mapping emissions that can be applied to the entire globe. High-emission pixels are readily seen in Fig. 7, and some of the pixels were attributed to pixels containing power plants. Because such emitting pixels are not indicated by maps based on population or nightlight data, the individual mapping of point sources is an advantage inherent in the procedure used in this study. Because the geographical coordinates of power plants were available in CARMA, this fine-scale mapping approach fully utilized location information with reasonably small dilution. In our opinion, the available information is insufficient to fully evaluate the relationship between CO_2 emissions and nightlight intensity. In addition, we cannot evaluate the extent to which emission intensities are reasonable at this global spatial

ACPD
10, 16307–16344, 2010

scale, as such information is only available for some individual countries, regions, or cities. Because the associated error usually increases at finer (higher) spatial resolutions, careful evaluation should be performed when utilizing the inventory presented in this study for atmospheric simulations. Regardless of such concerns, however, our high-resolution inventory may be applicable to global or regional high-resolution atmospheric simulations. In particular, one can perform, for example, atmospheric simulations with different spatial resolutions using a single consistent inventory. This inventory may also be applied toward interpreting the spatial variability in satellite CO_2 measurements globally.

3.3 Uncertainties

Here, we discuss the possible sources of uncertainties associated with our estimates. Our procedure may include three major sources of uncertainty: (1) the calculation of national and regional emissions, (2) the use of a point source database, and (3) the use of the nightlight surrogate distribution. The first source has already been discussed in the previous section. Therefore, we will discuss the second and third sources of error.

The use of a point source database is an appealing feature of the procedure presented in this paper. To our knowledge, there are no other power plant databases publicly available that cover the entire globe. This fact was the primary motivation for utilizing the CARMA database in our development. However, CARMA obviously does not cover all existing power plants worldwide, and the emission estimate was performed using limited data (Wheeler and Ummel, 2008). In addition, geographical coordinates provided by CARMA sometimes indicate false locations. One cause of these errors is the method for deriving coordinate information. The location of power plants was generally indicated by the plants postal address in the original public data or commercial subscription data. As the postal addresses were converted into coordinate information (latitude and longitude) via fuzzy matching using geographical information systems (Wheeler and Ummel, 2008), the addresses were sometimes erroneously assigned to places with the same name or a similar name. Apart from the CARMA

ACPD
10, 16307–16344, 2010

database, we extended the CARMA emissions for the year 2007 to the years 1980–2007 using national emission trends, under the assumption that the power plants had persistently contributed emissions over the intervening years. Therefore, uncertainties may increase in the years prior to 2006, which is actually the year 2007 in the CARMA database. Considering these points, uncertainties arising from the extrapolation of emissions may be larger than those associated with selection of the base year. With respect to the available spatial locations of power plants, we reviewed the coordinate information for 300 power plants in the CARMA data, one by one, using online resources, such as Google Earth (http://earth.google.com/) and Wikimapia (http://wikimapia.org/). In the sample set of 300 plants, which constitutes less than 3% of the fossil fuel power plants listed in the CARMA dataset, spatial errors were often present in Chinese power plants and sometimes in Indian plants. Great care must be taken with regards to the location of power plants when using the current version of ODIAC. The next version is expected to contain the corrected locations of the 300 power plants.

The use of nightlight data is an appealing feature of the present study. We determined the spatial distribution of the source regions by assuming that nightlight directly correlates with CO_2 emissions. Whereas this assumption is applicable to developed countries, it is not well suited for developing countries (e.g., Raupach et al., 2009). Saturated pixels were assigned the highest radiance pixel values for simplicity. It was assumed that the relationship between CO_2 emissions and nightlight was linear and uniform across the different countries, although the relationship may be strongly country-dependent. In addition, we applied one composite radiance data set to all years because of the limited availability of other radiance data sets. FFDAS utilized a specific annual composite nightlight data set for each year to compile the map for that year (Rayner et al., 2010). We expect that the spatial distribution may not be significantly influenced by the employed data set, because it is not reasonable to assume that many large cities may suddenly emerge or move over the course of two decades. We do expect significant errors to arise from changes in the light intensity, which may have changed significantly, especially in developing countries and regions.

ACPD
10, 16307–16344, 2010

4 Conclusions

We developed a global inventory of fossil fuel CO_2 emissions (the ODIAC) for the years 1980–2007 by combining information from the global power-plant database CARMA and a special product of the DMSP-OSL satellite nightlight data. In this study, we focused on the disaggregation of national emissions using these two key components. For this purpose, we only considered land-based CO_2 emissions, which are attributable to the combustion of fossil fuels. Emissions for international bunkers, fisheries, and gas flares were not considered due to their unique emission distribution and intensities. The nightlight map was a good predictor of the spatial distribution of potential source regions up to the city level, and fossil fuel power-plant emissions were placed directly at the locations indicated in the CARMA database. The resultant spatial distribution was somewhat different from that of previously described population-based inventories. Nightlight was expected to function as a comprehensive surrogate for regional unique sources, such as population and transportation networks, beyond the features originally attributed to nightlights. Our emission map was compared with the Vulcan inventory across the US for the year 2002 and with other existing global inventories. Our inventory showed better agreement with the Vulcan inventory than did other existing inventories, with respect to spatial patterns and absolute differences, at spatial resolutions that are suitable for regional flux inversions. The comparison suggested that the inclusion of point sources may be crucial for emission mapping at fine spatial scales. Apart from flux inversions, our inventory may benefit global and regional atmospheric simulations. However, a careful quantitative evaluation may be necessary when performing atmospheric simulations using this inventory. Although it is difficult to find a single comprehensive global tool for conducting detailed global evaluations, regional evaluations may be feasible. Emerging satellite CO_2 measurements may be applicable to such evaluations. Uncertainties associated with the estimates reported in this study may arise from the calculations of national and regional emissions, the accuracy of the point source database, and the use of nightlight maps as the only surrogate emission

ACPD
10, 16307–16344, 2010

map. These uncertainties are largely due to problems with data quality or availability, and they encompass the limitations associated with the development discussed here.

The primary motivating factor for this study was to provide a priori information on fossil fuel CO_2 emissions for flux inversions using observational data from GOSAT. We focused on fossil fuel CO_2 emissions on land. Other fossil fuel emissions that were not considered in this study, such as gas flares, international bunkers, and fisheries, may need to be accounted for by including such inventories in a full description of fossil fuel CO_2 emissions. The seasonal variations in fossil fuel emissions, as suggested in Gurney et al. (2005), may have an impact on flux estimates of inversions. In addition to annual emissions, gridded monthly emissions need to be developed for emerging monthly flux inversions. The derivation of monthly emission fields is currently under investigation.

Acknowledgements. This study was conducted as part of the GOSAT project promoted by the Japan Aerospace Exploration Agency (JAXA), the National Institute for Environmental Studies (NIES), Japan, and the Ministry of the Environment (MOE), Japan. Power plant data used in this study were taken from CARMA (CARbon Monitoring and Action, http://carma.org/). The nightlight data were obtained from US Air Force Defence Meteorological Satellite Project Operational Linescan System (DMSP-OSL) satellites processed and archived by The US National Oceanic Atmospheric Administration (NOAA) National Geophysical Data Center (NGDC). Population and national boundary data (GPWv3) were provided by the Trustees of Columbia University in the City of New York, the United Nations Food and Agriculture Programme (FAO), and the Centro Internacional de Agricultura Tropical (CIAT). The authors would like to thank Peter J. Rayner of LSCE for his contribution to the evaluation of our product and Stefan Reis of the University of Edinburgh for productive comments on this paper.

References

Andres, R. J., Marland, G., Fung, I., and Matthews, E.: A 1°×1° distribution of carbon dioxide emissions from fossil fuel consumption and cement manufacture, 1950–1990, Global Biogeochem. Cy., 10, 419–429, 1996. 16309, 16310

ACPD

10, 16307–16344, 2010

Andres, R. J., Boden, T. A., and Marland, G.: Annual Fossil-Fuel CO_2 Emissions: Mass of Emissions Gridded by One Degree Latitude by One Degree Longitude, Carbon Dioxide Information Analysis Center, Oak Ridge National Laboratory, US Department of Energy, Oak Ridge, Tenn., USA, doi:10.3334/CDIAC/ffe.ndp058.2009, available at: http://cdiac.ornl.gov/epubs/ndp/ndp058/ndp058_v2009.html (last access: 30 June 2010), 2009. 16324, 16340

Baker, D. F., Bousquet, P., and Bruhwiler, L.: TransCom 3 inversion intercomparison: impact of transport model errors on the interannual variability of regional CO_2 fluxes, 1988–2003, Global Biogeochem. Cy., 20, GB1002, doi:10.1029/2004GB002439, 2006. 16309

Belward, A. S., Estes, J. E., and Kline, K. D.: The IGBP-DIS global 1-km land-cover data set DISCover: a project overview, Photogramm. Eng. Rem. S., 65, 1013–1020, 1999. 16318

Boden, T. A., Marland, G., and Andres, R. J.: Global, Regional, and National Fossil-Fuel CO_2 Emissions., Carbon Dioxide Information Analysis Center, Oak Ridge National Laboratory, US Department of Energy, Oak Ridge, Tenn., USA, doi:10.3334/CDIAC/00001, available at: http://cdiac.ornl.gov/trends/emis/overview_2006.html (last access: 30 June 2010), 2009. 16320

BP: Statistical Review of World Energy, London, available at: http://www.bp.com/productlanding.do?categoryId=6929&contentId=7044622 (last access: 24 February 2009), 2007. 16313, 16314, 16315, 16320, 16335

Brenkert, A. L.: Carbon dioxide emission estimates from fossil-fuel burning, hydraulic cement production, and gas flaring for 1995 on a one degree grid cell basis, available at: http://cdiac.esd.ornl.gov/ndps/ndp058a.html (last access: 30 June 2010), 1998. 16309, 16310, 16325, 16337

Briggs, D. J., Gulliver, J., Fecht, D., and Vienneau, D. M.: Dasymetric modelling of small-area population distribution using land cover and light emissions data, Remote Sens. Environ., 108, 451–466, 2007. 16316

Chevallier, F., Engelen, R. J., and Peylin, P.: The contribution of AIRS data to the estimation of CO_2 sources and sinks, Geophys. Res. Lett., 32, L23801, doi:10.1029/2005GL024229, 2005. 16310

Chevallier, F., Bréon, F., and Rayner, P. J.: Contribution of the Orbiting Carbon Observatory to the estimation of CO_2 sources and sinks: theoretical study in a variational data assimilation framework, J. Geophys. Res., 112, D09307, doi:10.1029/2006JD007375, 2007. 16309

Cinzano, P., Falchi, F., Elvidge, C. D., and Baugh, K. E.: The artificial night sky brightness mapped from DMSP Operational Linescan System measurements, Mon. Not. R. Astron.

ACPD
10, 16307–16344, 2010

Soc., 318, 641–657, 2000. 16317
Doll, C. N. H., Muller, J.-P., and Elvidge, C. D.: Night-time imagery as a tool for global mapping of socioeconomic parameters and greenhouse gas emissions, Ambio, 29, 157–162, 2000. 16311, 16316
EC-JRC/PBL: Emission Database for Global Atmospheric Research (EDGAR), release version 4.0, available at: http://edgar.jrc.ec.europa.eu (last access: 30 June 2010), 2009. 16310, 16312, 16320, 16321, 16340
Elvidge, C. D., Baugh, K. E., Kihn, E. A., Kroehl, H. W., and Davis, E. R.: Mapping city lights with nighttime data from the DSMP operational linescan system, Photogramm. Eng. Rem. S., 63, 727–734, 1997. 16311, 16316
Elvidge, C. D., Baugh, K. E., Dietz, J. B., Bland, T., Sutton, P. C., and Kroehl, H. W.: Radiance calibration of DMSP-OLS low-Light imaging data of human settlements – a new device for portraying the Earth's surface entire, Remote Sens. Environ., 68, 77–88, 1999. 16316, 16317
Elvidge, C. D., Imhoff, M. L., Baugh, K. E., Hobson, V. R., Nelson, I., Safran, J., Dietz, J. B., and Tuttle, B. T.: Night-time lights of the world: 1994–1995, Photogramm. Eng. Rem. S., 56, 81–99, 2001. 16316
Elvidge, C. D., Baugh, K. E., Tuttle, B. T., Howard, A. T., Pack, D. W., Milesi, C., and Erwin, E. H.: A twelve year record of national and global gas flaring volumes estimated using satellite data, Final Report to the World Bank, available at: http://siteresources.worldbank.org/INTGGFR/Resources/DMSP_flares_20070530_b-sm.pdf (last access: 30 June 2010), 2007. 16317
Gregg, J. S., Andres, R. J., and Marland, G.: China: Emissions pattern of the world leader in CO_2 emissions from fossil fuel consumption and cement production, Geophys. Res. Lett., 35, 10288–10293, doi:10.1029/2007GL032887, 2007. 16313, 16319
Gurney, K. R., Rachel, L. M., Denning, A. S., Rayner, P. J., Baker, D., Bousquet, P., Bruhwiler, L., Chen, Y.-H., Ciais, P., Fan, S., Fung, I. Y., Gloor, M., Heimann, M., Higuchi, K., John, J., Maki, T., Maksyutov, S., Masarie, K., Peylin, P., Prather, M., Pak, B. C., Randerson, J., Sarmiento, J., Taguchi, S., Takahashi, T., and Yuen, C.-W.: Towards robust regional estimates of CO_2 sources and sinks using atmospheric transport models, Nature, 415, 626–630, 2002. 16309, 16325
Gurney, K. R., Chen, Y.-H., Maki, T., Kawa, S. R., Andrews, A., and Zhu, Z.: Sensitivity of atmospheric CO_2 inversions to seasonal and interannual variations in fossil fuel emissions, J. Geophys. Res., 110, D10308, doi:10.1029/2004JD005373, 2005. 16309, 16330
Gurney, K. R., Mendoza, D. L., Zhou, Y., Fischer, M. L., Miller, C. C., Geethakumar, S., and de la

ACPD
10, 16307–16344, 2010

Rue du Can, S.: High resolution fossil fuel combustion CO_2 emission fuxes for the united states, Environ. Sci. Technol., 43(14), 5535–5541, doi:10.1021/es900806c, 2009. 16311, 16324, 16325

Houweling, S., Hartmann, W., Aben, I., Schrijver, H., Skidmore, J., Roelofs, G.-J., and Breon, F.-M.: Evidence of systematic errors in SCIAMACHY-observed CO_2 due to aerosols, Atmos. Chem. Phys., 5, 3003–3013, doi:10.5194/acp-5-3003-2005, 2005. 16309

IEA: CO_2 emissions from fuel combustion: 1971–2005 (2007 edn.), International Energy Agency, Paris, 2007. 16309, 16314, 16320, 16340

IPCC: Revised 1996 IPCC Guidelines for National Greenhouse Gas Inventories, Tech. rep., IPCC/OECD/IEA, Paris, available at: http://www.ipcc-nggip.iges.or.jp/public/gl/invs1.html (last access: 30 June 2010), 1996. 16313, 16320

IPCC: Climate Change 2007: The Physical Science Basis, Cambridge University Press, Cambridge, UK, 2007. 16309

Marland, G. and Rotty, R. M.: Carbon dioxide emissions from fossil fuels: a procedure for estimation and results for 1950–82, Tellus B, 36, 232–261, 1984. 16320

Marland, G., Boden, T. A., and Andres, R. J.: Global, Regional, and National Fossil Fuel CO_2 Emissions, in: Trends: A Compendium of Data on Global Change, Carbon Dioxide Information Analysis Center, Oak Ridge National Laboratory, US Department of Energy, Oak Ridge, Tenn., USA, available at: http://cdiac.ornl.gov/trends/emis/overview.html(last access: 30 June 2010) 2008. 16309

Myhre, G., Alterskjær, K., and Lowe, D.: A fast method for updating global fossil fuel carbon dioxide emissions, Environ. Res. Lett., 4, 034012, doi:10.1088/1748-9326/4/3/034012, 2009. 16313

Ohara, T., Akimoto, H., Kurokawa, J., Horii, N., Yamaji, K., Yan, X., and Hayasaka, T.: An Asian emission inventory of anthropogenic emission sources for the period 1980–2020, Atmos. Chem. Phys., 7, 4419–4444, doi:10.5194/acp-7-4419-2007, 2007. 16324

Olivier, J. G. J., Aardenne, J. A. V., Dentener, F. J., Pagliari, V., Ganzeveld, L. N., and Peters, J. A. H. W.: Recent trends in global greenhouse gas emissions: regional trends 1970–2000 and spatial distribution of key sources in 2000, J. Integr. Env. Sci., 2(2–3), 81–99, doi:10.1080/15693430500400345, 2005. 16309, 16310

Raupach, M. R., Rayner, P. J., and Page, M.: Regional variations in spatial structure of nightlights, population density and fossil-fuel CO_2 emissions, Energ. Policy, 38(9), 4756–4764, doi:10.1016/j.enpol.2009.08.021, 2009. 16311, 16317, 16328

ACPD

10, 16307–16344, 2010

Rayner, P. J. and O'Brien, D. M.: The utility of remotely sensed CO_2 concentration data in surface source inversions, Geophys. Res. Lett., 28(1), 175-178, doi:10.1029/2000GL011912, 2001. 16309

Rayner, P. J., Raupach, M. R., Paget, M., Peylin, P., and Koffi, E.: A new global gridded dataset of CO_2 emissions from fossil fuel combustion: 1: Methodology and evaluation, J. Geophys. Res., accepted, 2010. 16311, 16317, 16325, 16328, 16337

Stephens, B. B., Gurney, K. R., Tans, P. P., Sweeney, C., Peters, W., Bruhwiler, L., Ciais, P., Ramonet, M., Bousquet, P., Nakazawa, T., Aoki, S., Inoue, T. M. G., Vinnichenko, N., Lloyd, J., Jordan, A., Heimann, M., Shibistova, O., Langenfelds, R. L., Steele, L. P., Francey, R. J., and Denning, A. S.: Weak northern and strong tropical land carbon uptake from vertical profiles of atmospheric CO_2, Science, 316, 1732–1735, doi:10.1126/science.1137004, 2007. 16309

Strow, L. L. and Hannon, S. E.: A 4-year zonal climatology of lower tropospheric CO_2 derived from ocean-only Atmospheric Infrared Sounder observations, J. Geophys. Res., 113, D18302, doi:10.1029/2007JD009713, 2008. 16310

UN: 2006 Energy Statistics Yearbook, Tech. rep., United Nations, Department for Economic and Social Information and Policy Analysis, Statistics Division, New York, 2008. 16320

Wheeler, D. and Ummel, K.: Calculating CARMA: Global Estimation of CO_2 Emissions From the Power Sector, available at: http://www.cgdev.org/files/16101_file_Calculating_CARMA_FINAL.pdf (last access: 30 June 2010), 2008. 16315, 16327

Yokota, T., Yoshida, Y., Eguchi, N., Ota, Y., Tanaka, T., Watanabe, H., and Maksyutov, S.: Global concentrations of CO_2 and CH_4 retrieved from GOSAT: First preliminary results, SOLA, 5, 160–163, doi:10.2151/sola.2009-041, 2009. 16310

ACPD

10, 16307–16344, 2010

High resolution global fossil CO_2 inventory

T. Oda and S. Maksyutov

Table 1. Definition of geographic regions in this study. This definition was adopted from BP (2007).

Region	Definition
North America	US (excluding Puerto Rico), Canada, Mexico
South and Central America	Caribbean (including Puerto Rico), Central and South America
Europe and Eurasia	European members of the OECD plus Albania, Bosnia-Herzegovina, Bulgaria, Croatia, Cyprus, Former Yugoslav Republic of Macedonia, Gibraltar, Malta, Romania, Serbia and Montenegro, Slovenia, and Former Soviet Union (Armenia, Azerbaijan, Belarus, Estonia, Georgia, Kazakhstan Kyrgyzstan, Latvia, Lithuania, Moldova, Russian Federation, Tajikistan, Turkmenistan, Ukraine and Uzbekistan)
Middle East	Arabian Peninsula, Iran, Iraq, Israel, Jordan, Lebanon and Syria
Africa	African continent
Asia and Pacific	Brunei, Cambodia, China, China Hong Kong SAR, Indonesia, Japan, Laos, Malaysia, Mongolia, North Korea, Philippines, Singapore, South Asia (Afghanistan, Bangladesh, India, Myanmar, Nepal, Pakistan, Sri Lanka), South Korea, Taiwan, Thailand, Vietnam, Australia, New Zealand, Papua New Guinea, Oceania.

ACPD
10, 16307–16344, 2010

Table 2. Summary of the national and regional annual emission estimates for the year 2006. "Code" in the second column refers to the standard country or area codes defined by the Statistical Division of the United Nations (http://unstats.un.org/unsd/methods/m49/m49.htm). National and regional emissions are shown in the national total ("total" in the third column), point source emission accompanied by the percentage of the national total ("point source" in the fourth column), and emissions from other sources ("other" in the last column). Values are reported in units of Mt CO_2/yr ([a]: Belgium includes Luxemburg. [b]: Administrative regions).

Country name	Code	Emissions (Mt CO_2/yr) Total	Point source	(%)	Other	Country name	Code	Emission (Mt CO_2/yr) Total	Point source	(%)	Other
United Arab Emirates	ARE	150	27	(17.7)	123	Republic of Korea	KOR	614	192	(31.3)	422
Argentina	ARG	153	32	(21.0)	121	Kuwait	KWT	70	13	(18.3)	57
Australia	AUS	403	224	(55.6)	179	Lithuania	LTU	16	1	(7.3)	15
Austria	AUT	74	16	(21.8)	58	Mexico	MEX	408	102	(25.0)	306
Azerbaijan	AZE	35	10	(28.8)	25	Malaysia	MYS	161	65	(40.6)	95
Belgium[a]	BEL	185	30	(16.4)	155	Netherlands	NLD	263	61	(23.2)	202
Bangladesh	BGD	48	12	(24.1)	37	Norway	NOR	41	1	(2.0)	40
Bulgaria	BGR	51	25	(47.9)	27	New	NZL	38	10	(25.2)	29
Belarus	BLR	62	14	(22.8)	48	Pakistan	PAK	134	25	(18.7)	109
Brazil	BRA	371	24	(6.4)	347	Peru	PER	25	5	(18.2)	20
Canada	CAN	630	172	(27.3)	458	Philippines	PHL	68	35	(50.7)	34
Switzerland	CHE	45	0.	(0.7)	45	Poland	POL	331	180	(54.5)	150
Chile	CHL	67	24	(35.3)	43	Portugal	PRT	67	25	(36.5)	43
China	CHN	6023	3117	(51.8)	2906	Qatar	QAT	52	8	(14.6)	44
Colombia	COL	57	9	(15.1)	48	Romania	ROU	103	0.	(0.0)	103
Czech	CZE	128	64	(50.0)	64	Russian	RUS	1681	478	(28.5)	1202
Germany	DEU	891	429	(48.1)	462	Saudi	SAU	436	71	(16.2)	366
Denmark	DNK	61	25	(41.0)	36	Singapore	SGP	148	15	(9.8)	133
Algeria	DZA	88	17	(18.9)	71	Slovakia	SVK	39	11	(27.2)	28
Ecuador	ECU	24	3	(11.5)	22	Sweden	SWE	62	3	(4.6)	59
Egypt	EGY	152	42	(27.5)	110	Thailand	THA	231	77	(33.3)	154
Spain	ESP	382	152	(39.7)	230	Turkmenistan	TKM	54	5	(9.9)	48
Finland	FIN	62	32	(51.9)	30	Turkey	TUR	272	100	(37.0)	171
France	FRA	423	53	(12.6)	370	Taiwan[b]	TWN	338	137	(40.5)	201
United	GBR	607	227	(37.4)	380	Ukraine	UKR	345	73	(21.3)	272
Greece	GRC	106	50	(47.1)	56	United States	USA	6411	2808	(43.8)	3603
Hong Kong[b]	HKG	79	0.	(0.0)	79	Uzbekistan	UZB	112	31	(27.2)	82
Hungary	HUN	61	16	(26.1)	45	Venezuela	VEN	139	12	(8.7)	127
Indonesia	IDN	332	91	(27.4)	241	South Africa	ZAF	450	218	(48.5)	232
India	IND	1220	638	(52.2)	583						
Ireland	IRL	46	17	(38.4)	28	North America	–	0.	0.	–	0.
Iran	IRN	466	82	(17.6)	384	South and Cent. America	–	253	24	(9.6)	229
Iceland	ISL	3	0.	(0.5)	3	Europe and Eurasia	–	196	63	(32.0)	133
Italy	ITA	495	168	(33.9)	327	Middle East	–	330	80	(24.2)	250
Japan	JPN	1371	414	(30.2)	957	Africa	–	281	57	(20.2)	225
Kazakhstan	KAZ	189	60	(31.6)	129	Asia Pacific	–	245	26	(10.8)	219

ACPD
10, 16307–16344, 2010

Table 3. Comparison, across the US, of our map and the Vulcan map. "Brankert 1998" (the first column) is a population-based map constructed at 1° resolution (Brenkert, 1998). "FFDAS" (the second column) was based on nightlight data corrected by population data (Rayner et al., 2010). The total emissions of the participating inventories were scaled with respect to the Vulcan total emission level for the year 2002, and the absolute differences (diff) and spatial correlations (corr) with the Vulcan map were calculated at different spatial aggregation levels (0.5–4°) (Rayner et al., 2010). Values are given in units of Megatonne carbon.

Resolution	Brenkert 1998		FFDAS		ODIAC	
(°)	diff (Mt C)	corr	diff (Mt C)	corr	diff (Mt C)	corr
0.5	–	–	1143	0.74	744	0.87
1.0	1045	0.75	900	0.85	474	0.94
2.0	788	0.84	651	0.91	315	0.97
3.0	654	0.87	545	0.92	262	0.98
4.0	644	0.87	479	0.93	206	0.99

ACPD
10, 16307–16344, 2010

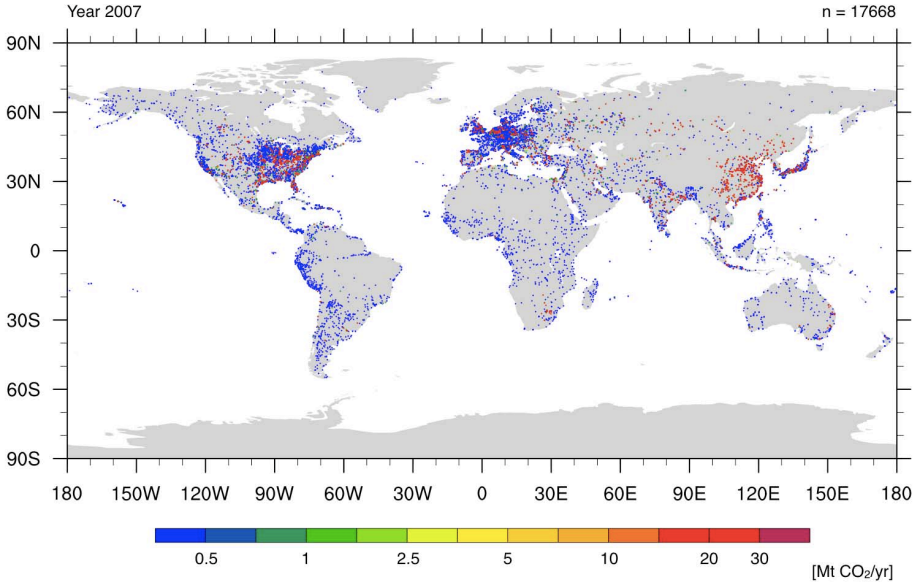

Fig. 1. Global spatial distributions of power plant emissions for the year 2007. The coordinate and emission data of power plants were taken from the CARMA database (CARbon Monitoring and Action, http://carma.org/). Power plant data with invalid coordinate information and no CO_2 emissions were excluded, and the 17 668 power plants incorporated into our inventory were plotted. Values are given in units of Mt CO_2/yr.

ACPD
10, 16307–16344, 2010

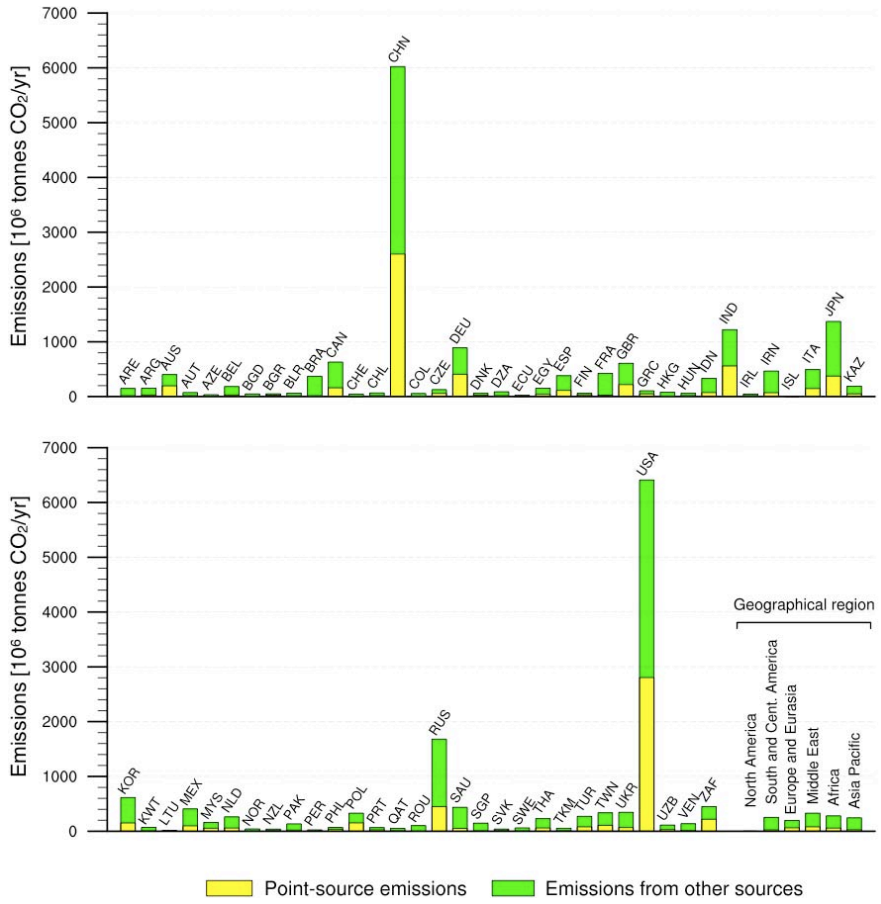

Fig. 2. National and regional total emission estimates for the year 2006. The yellow portion indicates emissions from point sources, and green indicates emissions from other sources (non-point). National and regional total point-source emissions (yellow) were calculated using the CARMA power plant data shown in Fig. 1. The non-point source emissions (green) were estimated by the simple residual of the total emission minus the point source emissions. Values are given in units of Mt CO_2/yr.

ACPD
10, 16307–16344, 2010

High resolution global fossil CO_2 inventory

T. Oda and S. Maksyutov

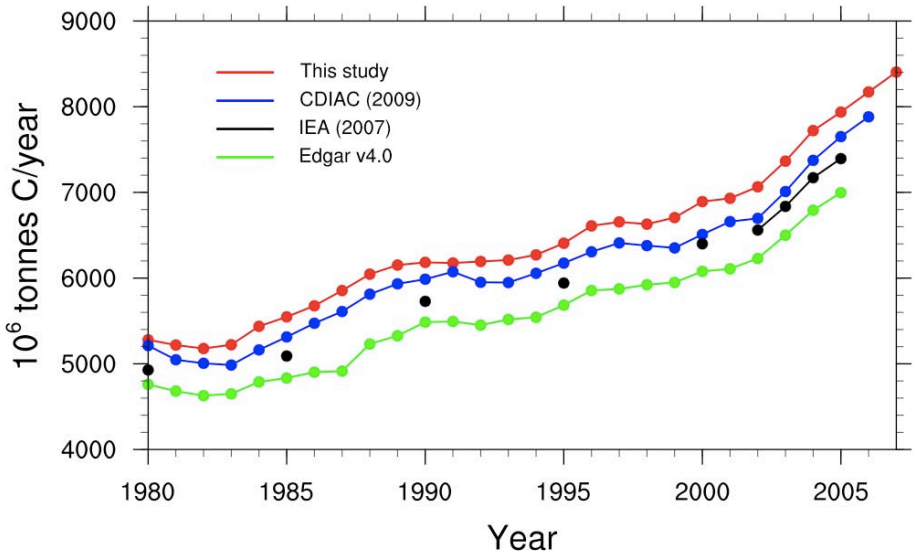

Fig. 3. Comparison of the historical global CO_2 emission estimates for the years 1980–2007. The red line shows the estimates of this study (ODIAC), blue indicates CDIAC (Andres et al., 2009) estimates (excluding cement production), black indicates IEA (IEA, 2007) estimates, and green indicates EDGAR v4.0 (EC-JRC/PBL, 2009) estimates. Values are given in units of Mt C/yr.

ACPD
10, 16307–16344, 2010

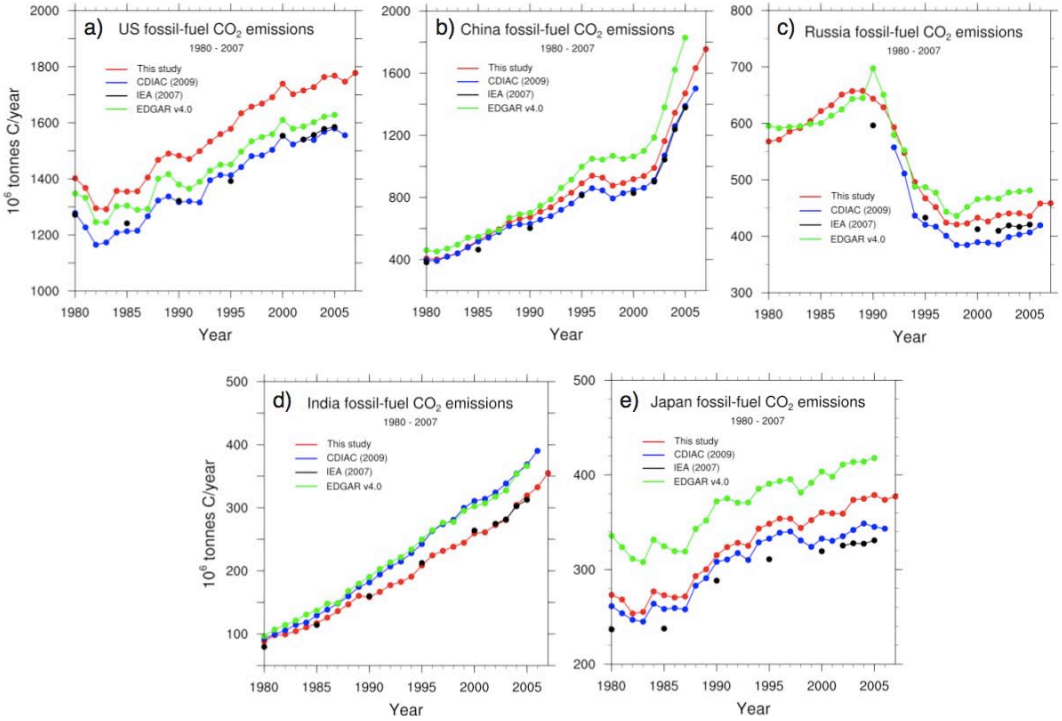

Fig. 4. Comparison of historical CO_2 emission estimates (1980–2007) for the five top emitting countries. **(a)** United States, **(b)** China, **(c)** Russian Federation, **(d)** India, and **(e)** Japan. The color attribution is the same as in Fig. 3. Values are given in units of Mt C/yr.

ACPD
10, 16307–16344, 2010

High resolution global fossil CO_2 inventory

T. Oda and S. Maksyutov

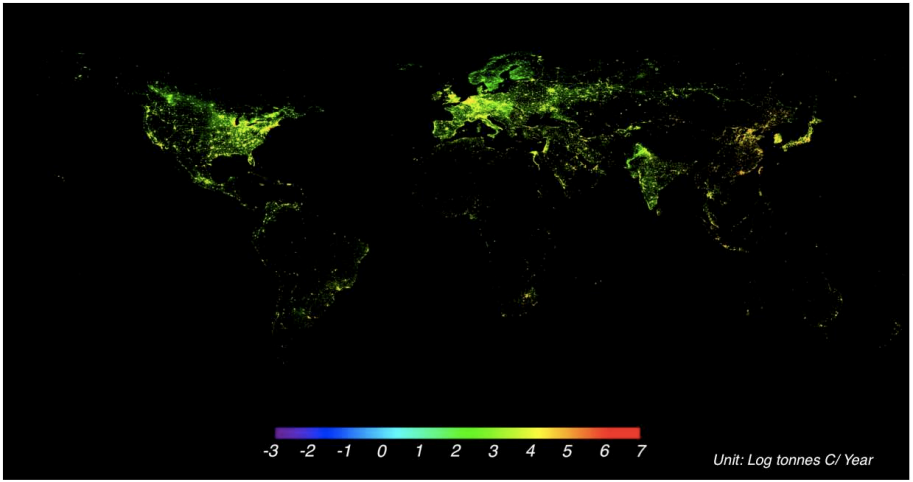

Fig. 5. Global distribution of total CO_2 emissions for the year 2006. The map was drawn using a reduced 5-km-resolution ODIAC inventory; therefore, the actual size of each pixel is 5 km×5 km. Values are given in units of the log (base 10) of tonnes carbon 5 km^{-2} $year^{-1}$.

ACPD
10, 16307–16344, 2010

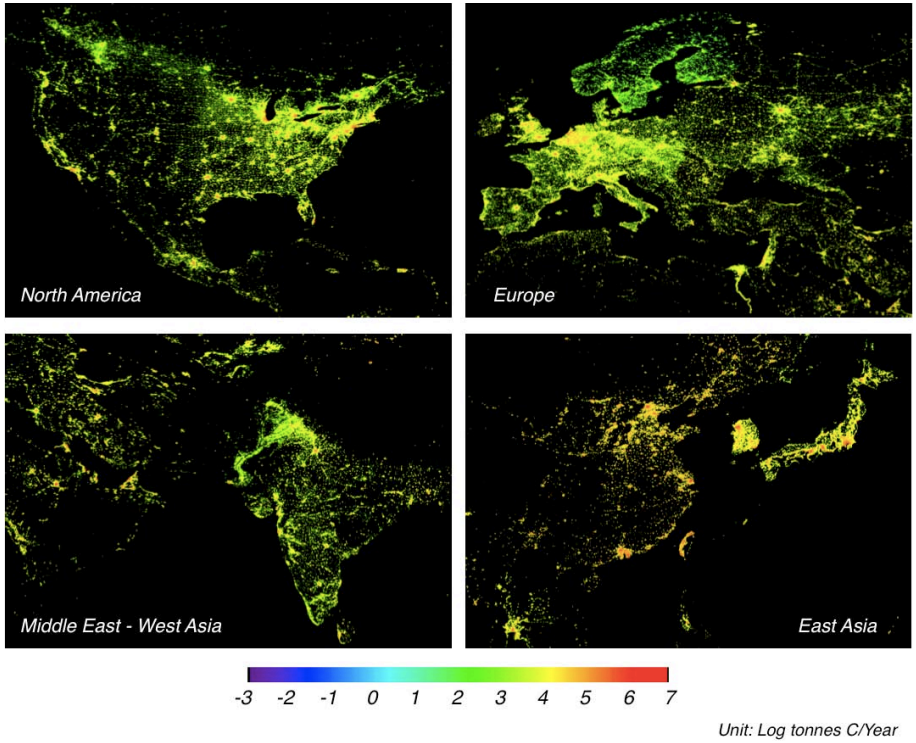

Fig. 6. Regional spatial distributions of CO_2 emissions for the year 2006. From top left (clockwise): North America, Europe, East Asia, and the Middle East and West Asia. The maps shown here were drawn using reduced 5-km-resolution ODIAC inventory on the same scale. Values are given in units of the log (base 10) of tonnes carbon 5 km^{-2} $year^{-1}$. Note that the maps are drawn in different scales.

ACPD
10, 16307–16344, 2010

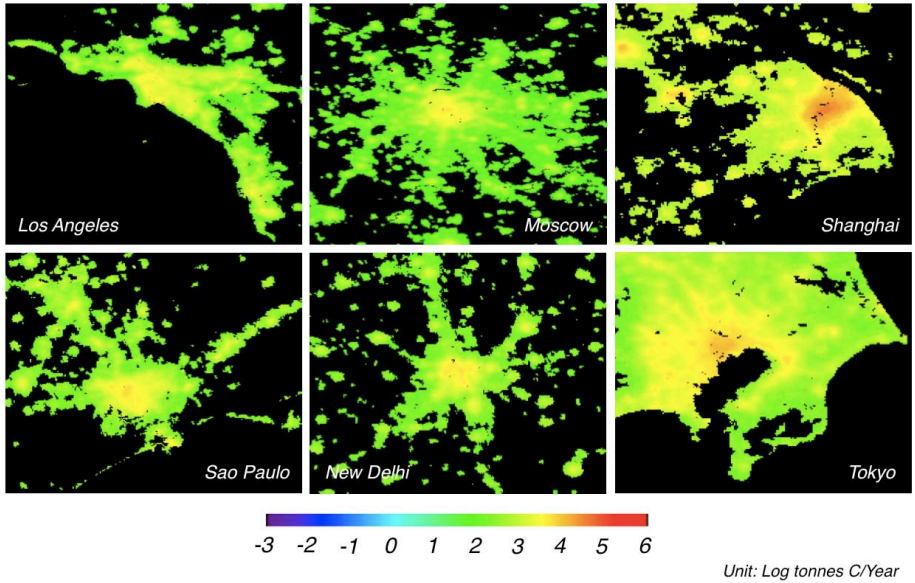

Fig. 7. Spatial distributions of CO_2 emissions over heavily populated cities worldwide for the ear 2006. From top left (clockwise): Los Angeles, Moscow, Shanghai, Tokyo, New Delhi, and Sao Paulo. The maps were drawn using the original 1-km-resolution ODIAC inventory; therefore, the actual size of each pixel is 1 km×1 km. Values are given in units of the log (base 10) of tonnes carbon 1 km^{-2} $year^{-1}$. Note that the maps are drawn in different scales.

ACPD
10, 16307–16344, 2010